The optimal height of the synaptic cleft

Leonid P. Savtchenko[†‡] and Dmitri A. Rusakov[†§]

[†]Institute of Neurology, University College London, Queen Square, London WC1N 3BG, United Kingdom; and [‡]Dnepropetrovsk National University, Dnepropetrovsk 49050, Ukraine

Edited by Charles F. Stevens, The Salk Institute for Biological Studies, La Jolla, CA, and approved December 4, 2006 (received for review August 2, 2006)

Signal integration in the brain is determined by the size and kinetics of rapid synaptic responses. The latter, in turn, depends on the concentration profile of neurotransmitter in the synaptic cleft. According to a traditional view, narrower clefts should correspond to higher intracleft concentrations of neurotransmitter, and therefore to the enhanced activation of synaptic receptors. Here, we argue that narrowing the cleft also increases electrical resistance of the intracleft medium and therefore reduces local receptor currents. We employ detailed theoretical analyses and Monte Carlo simulations to propose that these two contrasting phenomena result in a relatively narrow range of cleft heights at which the synaptic receptor current reaches its maximum. Over a physiological range of synaptic parameters, the ''optimum'' height falls between ≈12 and 20 nm. This range is consistent with the structure of central synapses reported by electron microscopy. Therefore, our results suggest that a simple fundamental principle may underlie the synaptic cleft architecture: to maximize synaptic strength.

AMPA receptor | diffusion | glutamate | Monte Carlo | neural communication

The waveform of rapid synaptic responses shapes the temporal domain of signal integration in the brain (1, 2). In turn, the kinetics of synaptic receptor currents is constrained by diffusion of neurotransmitter in the synaptic cleft (3, 4). This relationship, however, remains poorly understood, mainly because events inside the cleft are beyond the powers of direct experimental observation. There is little doubt, however, that synaptic cleft geometry is an important factor in shaping synaptic currents (3, 5–7). The straightforward logic of physics predicts that decreasing the cleft height should increase the intracleft concentration of neurotransmitter and therefore enhance activation of synaptic receptors (8). In turn, increasing the lateral cleft size could generally slow down neurotransmitter escape from the cleft and thus prolong synaptic responses (9). Indeed, faster AMPA receptor-mediated EPSCs have recently been associated with smaller synaptic apposition zones in the developing cerebellar synapses (10). However, lateral dimensions of synapses fluctuate considerably (even within homogeneous synaptic populations), whereas the cleft height remains remarkably stable. For instance, at the common excitatory synapses in hippocampal area CA1, the lateral cleft area varies several-fold (11) whereas the cleft height shows the coefficient of variation (an upper estimate) of only ≈26% (12). Interestingly, osmotic challenge or other physiological manipulations that affect dramatically the overall extracellular space dimensions (13, 14) do not appear to modify the synaptic cleft height (15). This parameter also remains virtually unchanged during development (16–18). Remarkably, in electron micrographs of synaptosomes (a preparation obtained using strong mechanical forces of centrifugal separation), the distance between the apposing synaptic membranes is indistinguishable from that in the intact neuropil. Across many synaptic types, this distance lies within a relatively narrow range of 15–25 nm (19), which appears to be determined by the rigid structure of the intracleft protein scaffolding (20–22). However, the adaptive purpose for the synaptic cleft height to be within this range is not clear: in theory, narrower cleft should provide for chemical synaptic transmission that is more efficient.

It has long been suggested, however, that the electric impedance of narrow synaptic clefts may reduce synaptic currents in the neuromuscular junction (23). A similar phenomenon has been proposed to occur in central synapses (24). Could this counterbalance the effects of the increased neurotransmitter concentration in narrow clefts? Here we use theoretical analyses and Monte Carlo simulations to investigate how the synaptic cleft height affects neurotransmitter diffusion, the electric resistance of the intracleft medium and, ultimately, synaptic receptor currents at a common excitatory synapse. We find that, over a physiological range of synaptic parameters, synaptic currents peak when the effective cleft height falls between ≈12 and 20 nm. This range is consistent with that reported by electron micrographs of central synapses. The results therefore suggest that the cleft architecture could be based on a simple principle: to maximize the strength of synaptic transmission.

Results

Synaptic Current Versus Cleft Height: A Convergent Analytical Solution. To obtain proof of principle, we first sought to evaluate the relationship between synaptic responses and the cleft height using basic laws of physics. According to the common approximation, synaptic clefts can be represented by a flat cylinder of radius R and height $\delta \ll R$ surrounded by an infinite three-dimensional medium (Fig. 1*A*). Rapid release of Q neurotransmitter molecules in the cleft center gives rise to the concentration profile

$$C(r, t, Q, D, \delta), \qquad [1]$$

where variables r and t stand, respectively, for the radial distance and time and D is the effective diffusion coefficient. The explicit form of $C(r, t, Q, D, \delta)$, which is a solution of the fundamental diffusion equation, indicates that concentration is simply inversely proportional to the cleft height δ (expressions **A1.2** and **A1.3**, *Appendix 1*).

Fast signaling in central synaptic circuits relies in large part on rapid activation of synaptic AMPA receptors by the excitatory neurotransmitter glutamate. This reaction involves complex multistage kinetics of receptor binding, activation, and desensitization (25–27). Because another major glutamate receptor type, NMDA, contributes negligibly to the peak amplitude of fast excitatory signals in baseline conditions (near the cell resting potential), we focused on the AMPA receptor responses only. To obtain a convergent analytical solution for the receptor kinetics, we used a reduced kinetic scheme that nonetheless provides

Author contributions: L.P.S. and D.A.R. designed research; L.P.S. performed research; D.A.R. analyzed data; and L.P.S. and D.A.R. wrote the paper.

The authors declare no conflict of interest.

This article is a PNAS direct submission.

Freely available online through the PNAS open access option.

[§]To whom correspondence should be addressed. E-mail: d.rusakov@ion.ucl.ac.uk.

This article contains supporting information online at www.pnas.org/cgi/content/full/0606636104/DC1.

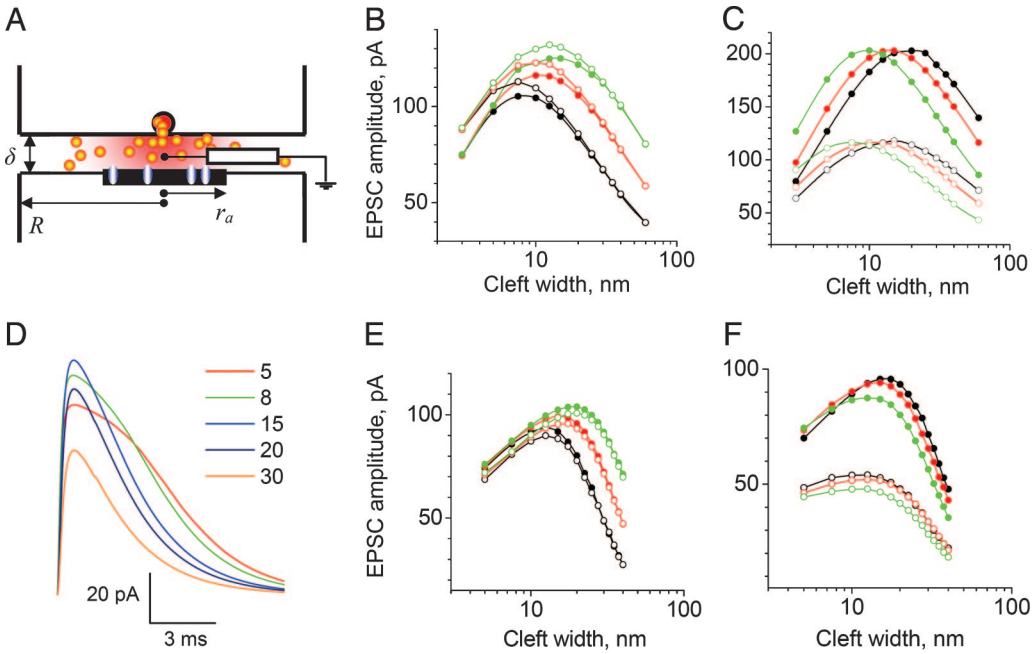

Fig. 1. Every synapse may have a unique cleft height at which the EPSC peaks. (*A*) Modeled synaptic environment, central cross-section: glutamate (yellow dots, red shade) released instantaneously in the cleft centre diffuses inside the synaptic apposition zone (radius *R*) before escaping into the surrounding space. Activation of AMPA receptors (blue ovals; randomly distributed within the active zone of radius r_a) generates an ion current attenuated by the volume-conductor resistance (depicted) of the intracleft medium. (*B* and *C*) Theoretical analyses predict that, depending on the synaptic environment, the current amplitude peaks at a unique value of the synaptic cleft height δ. Open and filled circles, respectively (see *Appendix 5* for symbols and notations): $R = 150$ and 300 nm in *B* and $n = 100$ and 200 in *C*; black, red and green symbols/lines: $Q = 3{,}000$, 5,000, and 8,000 in *B*, and $D = 0.2$, 0.3, and 0.5 μm^2/ms in *C*. (*D–F*) Random-walk Monte Carlo simulations of glutamate molecule movements also predict a single-maximum relationship between synaptic currents and the cleft height. (*D*) Examples of simulated AMPA receptor EPSCs at different values of the cleft height δ (in nm, shown by colors); parameters: $Q = 3{,}000$; $D = 0.2$ μm^2/ms, $R = 300$ nm, $r_a = 70$ nm, $n = 120$. (*E* and *F*) AMPA receptor EPSCs peak at a unique value of δ. Open and filled circles, respectively: $R = 150$ and 300 nm (*E*) and $n = 50$ and 100 (*F*); black, red and green lines/symbols, respectively: $Q = 3{,}000$, 5,000, and 8,000 (*E*) and $D = 0.2$, 0.3, and 0.5 μm^2/ms (*F*).

reasonable approximation of receptor currents (expression **A2.1**, *Appendix 2*). Assuming that N ($\ll Q$) AMPA receptors are uniformly distributed within the postsynaptic active zone of radius r_a (Fig. 1*A*), receptor binding has little effect on the glutamate concentration time course (28). Indeed, in the typical small excitatory synapse, ≈3,000 neurotransmitter molecules interact with only several dozens of intracleft receptors. Another useful simplification is to calculate receptor currents based on the average glutamate concentration within the synaptic active zone radius ($r < r_a$; expression **A1.4**, *Appendix 1*). In this case, the time course of receptor opening probability P_o (fraction of open receptors) follows a convergent analytical expression (**A2.3**, *Appendix 2*). Quite expectedly, this expression predicts that the receptor opening probability increases as the cleft height δ decreases, as demonstrated earlier in a Monte Carlo model of a small excitatory synapse (8).

At the same time, however, δ determines the electrical resistance of the volume conductor represented by the extracellular medium inside the cleft. In the typical central synapse, the intracleft resistance could give rise to a significant voltage drop in the radial direction across the cleft, which in turn influences the local membrane potential $V(r)$ (24). The receptor channel current could therefore depend on how far the activated receptor is located with respect to the cleft center/edge. This follows the classical relationship $I(r) = \gamma(V(r) - V_{rev})$, where $V(r)$ is the local membrane potential and V_{rev} is the receptor reversal potential. The profile of $V(r)$ is determined by the cleft dimensions (R, r_a, δ) and by the extracellular medium resistivity R_{ex} (**A3.4**, *Appendix 3*). According to the basics of physics, the value of R_{ex} can be directly related to intracleft diffusivity D (**A3.3**, *Appendix 3*). Once the profile of $V(r)$ and the receptor opening probability have been determined, the total synaptic current $I_{syn}(t)$ can be obtained through integration over all receptors within the active zone

$$I_{syn}(t) = \frac{2\gamma N P_o(t)}{r_a^2} \int_0^{r_a} (V(r) - V_{rev}) r dr, \qquad [2]$$

where $P_o(t)$ reflects the adopted average P_o over the active zone (see above).

Substituting the respective functions into expression **2** yields a complex factor, which determines the total receptor current when $NP_o(t)$ receptors are activated (24)

$$I_{syn}(t) = V_o \frac{2\pi\delta}{R_{ex}} \frac{L(t)}{L(t)Ln(R/r_a) + J_0(L(t))/J_1(L(t))}. \qquad [3]$$

Here, V_o stands for the postsynaptic resting membrane potential outside the cleft, J_0 and J_1 denote Bessel functions of the first kind, and $L(t) = (NP_o(t)R_{ex}\gamma/\pi\delta)^{1/2}$. When $L(t)$ tends to zero, thus implying no detectable voltage drop along the cleft radius, expression **3** degrades into the classical case: $I_{syn}(t) = V_o NP_o(t)\gamma$.

Combining Eqs. **A1.2**, **A2.3**, and **3** above gives a complex expression for I_{syn} incorporating, respectively, glutamate diffusion, AMPA receptor activation, and current losses in the cleft. These derivations allow analytical testing of the relationship between the cleft height and the amplitude of synaptic currents for a variety of synaptic architectures.

Synaptic Parameters Explored. Clearly, conclusions drawn from a synaptic modeling study only make sense if the parameters

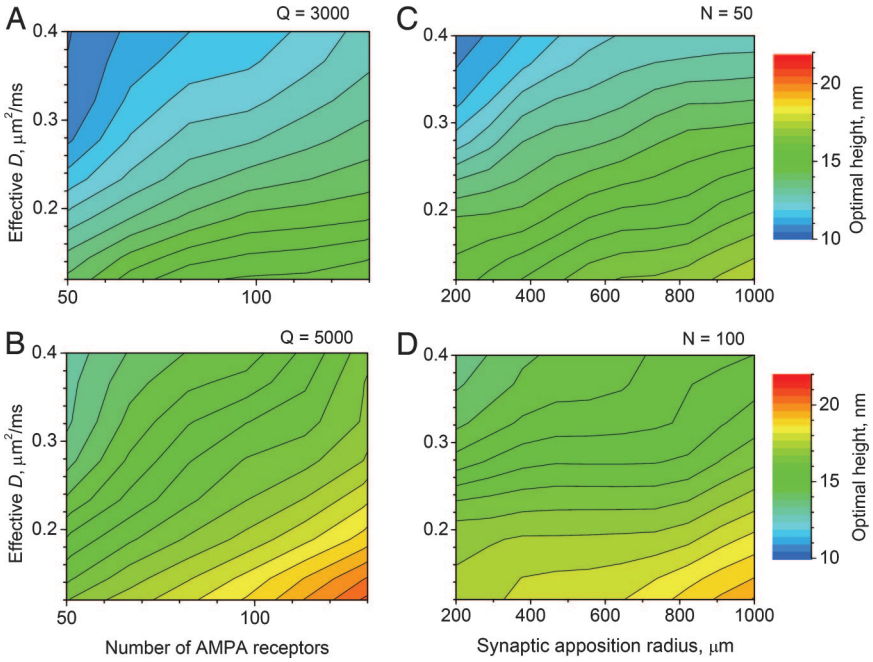

Fig. 2. A variety of synaptic architectures corresponds to a relatively narrow range of the optimal cleft heights. Color indicates the cleft height (pseudocolor scales on the right) at which the synaptic current reaches its maximum, as calculated over a wide range of synaptic parameters. (*A* and *B*) Varying the intracleft diffusion coefficients of glutamate *D* (ordinate) and the number of synaptic AMPA receptors *N* (abscissa) at two characteristic numbers of released glutamate molecules (*Q* = 3,000 and 5,000, as indicated). (*C* and *D*) Varying the diffusion coefficients of glutamate (ordinate) and the lateral synaptic dimensions (synaptic apposition zone radius *R*, abscissa) at two characteristic numbers of synaptic AMPA receptors (*n* = 50 and 100, as indicated).

involved either are constrained by experimental data or represent a plausible physiological range for the synapse in question. Therefore, we first assessed R_{free} (*Appendix 3*) by measuring resistivity of the gassed (95% O_2/5% CO_2) bath solution that we routinely use in physiological experiments in brain slices (29). The value we obtained using a Hash Lange meter HQ14d (probe CDC401–01) at 36–37°C was 59 ± 1 Ohm·cm [mean ± SD; supporting information (SI) Fig. 3], which is in good agreement with the temperature-dependent R_{free} values reported in refs. 30 and 31. Diffusivity of glutamate in the synaptic cleft was reported to decrease ≈3-fold compared with the free medium, from D_{free} ≈ 1.0 μm^2/ms to $D \approx 0.33$ μm^2/ms at physiological temperature (7). To cover the plausible physiological range of values, we therefore explored D from 0.15 to 0.5 μm^2/ms while adopting R_{free} = 59 Ohm·cm; these parameters in turn determined R_{ex} (*Appendix 3*). The synaptic active zone radius was set at 70 nm, and the number of available AMPA receptors varied from 50 to 120, in accordance with the detailed experimental description of the common glutamatergic synapses in area CA1 of the hippocampus (32–34). Similarly, the number of glutamate molecules released into the cleft was varied from the baseline value of 3,000 (35) to 8,000, to reflect the possibility of multivesicular release at this synaptic type (36). Finally, the lateral size of the synaptic apposition was varied 5-fold (between 200 and 1,000 nm), to reflect the high variability, including age-dependence, of the overall synaptic dimensions (10–12, 19). Within this range of synaptic parameters, the theoretical calculations described above predict that the maximum amplitude of synaptic current I_{syn} peaks when δ falls between ≈10 and 20 nm (Fig. 1 *B* and *C*).

Synaptic Current Versus Cleft Height: Monte Carlo Simulations. Based on fundamental laws of physics, the above derivations suggest that the cleft height could in principle optimize synaptic strength. However, to allow convergent analytical solutions, our theory had to rely on several simplifying assumptions (*Appendices 1–3*). To test whether similar phenomena take place in more realistic conditions, we extended our testing by employing a Monte Carlo model of the synaptic environment. In the model, individual glutamate molecules performed three-dimensional random-walk movements interacting with individual receptors (*Appendix 4*). When 3,000 or more glutamate molecules were released in the cleft center, the model generated plausible AMPA receptor-mediated currents (Fig. 1*D*), in line with those expected at the postsynaptic site of hippocampal neurons (37). Again, we tested the effect of the synaptic cleft height on the amplitude of AMPA receptor EPSCs over a plausible range of physiological parameters (see above). The results of Monte Carlo simulations suggest that I_{syn} at the typical small synapse peaks when the cleft height value falls between ≈12 and 20 nm depending on the synaptic environment (Fig. 1 *E* and *F*). These values are generally consistent with the range obtained in analytical computations (Fig. 1 *B* and *C*) in which the receptor kinetics scheme was truncated (*Appendix 2*) for the sake of convergent solutions.

To obtain a more comprehensive picture of the relationship between the optimal cleft height and synaptic architecture, we carried out a series of Monte Carlo simulations while systematically varying parameters of the synaptic environment. The results (Fig. 2) indicate that the optimal cleft height falls within a relatively narrow range of values, between ≈12 and 20 nm, across the variety of synaptic architectures characteristic for small excitatory synapses.

Discussion

It has commonly been assumed that the synaptic cleft height merely determines the effective concentration of released neurotransmitter, thus affecting synaptic strength in a monotonic fashion (8). However, a recent theoretical investigation suggested that narrowing the cleft could significantly increase the effective cleft resistance. thus reducing the synaptic current (24), in line with the classical conjecture by Eccles (23). The present study investigates how these two phenomena interact, concluding that the synaptic cleft height may have an adaptive function of optimizing synaptic strength.

Physiological experiments that would test this hypothesis directly are likely to be difficult because the rigid cleft structure appears to withstand various experimental manipulations, including physical separation of the synaptic membrane fraction or even the solubilization of the neighboring membranes (21). Indeed, electron micrographs obtained with different tissue fixation methods suggest a relatively constant average distance between pre- and postsynaptic membranes ranging between 15 and 25 nm (19, 22). The molecular basis of this architecture appears to rely on cadherin-type adhesion molecules that provide transcellular structural scaffolding connecting pre- and postsynaptic membranes (20, 21). Even if experimental modification of the cleft height was feasible, it would be difficult to verify any change on the scale of nanometers. In addition, the intracleft lumen contains a dense matrix of glyco-carbohydrates as well as extracellular domains of integral proteins protruding from the plasma membrane over several nanometers. Because these macromolecular structures are likely to reduce the volume available to the free movement of ions inside the cleft, the effective cleft height is likely to be smaller than the intermembrane distance routinely observed in an electron microscope. This could explain why the optimal cleft heights predicted by our simulations (Fig. 2) tend to be somewhat lower than the commonly observed intermembrane gap of 15–25 nm.

Importantly, our simulations suggest that the optimal cleft height could vary, albeit within a relatively narrow range, depending on the synaptic architecture (Fig. 2). In fact, many central synapses undergo age- or use-dependent modifications of synaptic efficacy. This often involves changes in synaptic morphology, in the amount of released neurotransmitter or in the number of available receptors (38–40). Does the synaptic cleft height change in these circumstances? Electron microscopy has thus far been unable to provide an answer to this question because the expected small range of change (few nanometers) is comparable with or less than the measurement error involved. Irrespective of the answer, however, our present results suggest that central synapses tend to have the cleft height that may help generate the largest synaptic response. If so, this might reflect a simple, yet previously unrecognized rule of synaptic architecture: "maximum effect at minimum expense."

Materials and Methods

Appendix 1: Analytical Solutions for Rapid Diffusion Inside the Cleft. Diffusion in the infinite two-dimensional flat cleft follows the fundamental diffusion equation expressed in cylindrical coordinates as

$$\frac{\partial C}{\partial t} = D\,\frac{1}{r}\,\frac{\partial}{\partial r}\left(r\,\frac{\partial C}{\partial r}\right), \qquad \textbf{[A1.1]}$$

where C, r, and D stand for concentration, radial distance, and diffusion coefficient, respectively. An instantaneous release of Q glutamate molecules in the cleft center gives rise to the concentration profile $C(r, t, Q, D, \delta)$

$$C(r,\,t,\,Q,\,D,\,\delta) = \frac{Q}{4\pi\delta Dt}\,\exp\left(-\frac{r^2}{4Dt}\right), \qquad \textbf{[A1.2]}$$

where δ stands for the cleft height. However, the dwell-time of glutamate molecules inside the two-dimensional cleft tends to be overestimated compared with that in real three-dimensional synapses (9). Therefore, we calculated diffusion profile for the cleft which opens into an infinite three-dimensional medium at the distance R from the cleft center, by introducing an absorbing boundary at $r = R$. Solving **A1.1** with this boundary condition gives a complex classical solution represented by a series of Bessel's functions (denoted J_0 and J_1):

$$C(r,\,t) = \frac{Q}{\delta\pi R^2}\,\sum_{i=1}^{\infty}\,\frac{J_0\left(\frac{\mu(i)r}{R}\right)}{J_1^2(\mu(i))}\,\exp\left(-\frac{\mu(i)Dt}{R^2}\right), \qquad \textbf{[A1.3]}$$

where $\mu(i) = \pi\,(i - 1/4 + 0.05661/(4i - 1) - (0.053/(4i - 1)^2)) + \ldots$). The difference between the concentration profiles calculated from **A1.2** and **A1.3** during the first 0.5 ms after release (the time window of the synaptic current peak) was, however, $<5\%$ (data not shown). For the sake of clarity, we therefore used solution **A1.2**.

Expressions **A1.2** and **A1.3** indicate that $C(r, t)$ is inversely proportional to the cleft height δ. Based on **A1.2**, the average glutamate concentration C^* within the active zone of radius r_a follows the expression

$$C^*(r_a,\,\delta,\,t) = \frac{Q}{\pi\delta r_a^2}\left(1-\exp\left(-\frac{r_a^2}{4Dt}\right)\right). \qquad \textbf{[A1.4]}$$

We used expression **A1.4** to calculate the average glutamate concentration that drives the opening kinetics of AMPA receptors within the synaptic active zone.

Appendix 2: AMPA Receptor Kinetics. The reduced kinetic scheme of AMPA receptor activation was

$$2Glu + AR \underset{k_{off}}{\overset{k_{on}}{\rightleftharpoons}} Glu_2AR \underset{\beta}{\overset{\alpha}{\rightleftharpoons}} O, \qquad \textbf{[A2.1]}$$

where Glu denotes one glutamate molecule, AR is AMPA receptor, O indicates the receptor channel open state, and α and β are the rates of channel opening and closing, respectively.

In accordance with scheme **A2.1**, we calculated the fraction of open AMPA receptors P_o using the set of differential equations

$$\begin{aligned}\frac{\partial[AR]}{\partial t} &= -2k_{on}C[AR] + k_{off}[Glu_2AR]\\ \frac{\partial[Glu_2AR]}{\partial t} &= 2k_{on}C[AR] - (k_{off} + \alpha)[Glu_2AR]\\ &\quad + \beta(1 - [AR] - [Glu_2AR]),\end{aligned} \qquad \textbf{[A2.2]}$$

where C is glutamate concentration, brackets denote concentrations of the corresponding compounds, as indicated, and the initial conditions ($t = 0$) are: $[AR] = 1$, $[Glu_2AR] = 0$.

With the four known parameters $k_{on} = 10\ \mathrm{mM^{-1}\ ms^{-1}}$, $k_{off} = 5\ \mathrm{ms^{-1}}$, $\alpha = 5\ \mathrm{ms^{-1}}$, and $\beta = 1\ \mathrm{ms^{-1}}$ incorporated as their numerical values (for the sake of clarity), the fraction of open receptors, $P_o = 1 - [AR] - [Glu_2AR]$, follows the expression (experimental values are rounded to two digits)

$$\begin{aligned}P_o(t) = {} & (10C\,\exp\left(-\frac{t}{2}\,(11 + 20C + \sqrt{T})\right)\\ & \times (11 - \sqrt{T} - (11 - \sqrt{T}) \times \exp(t\,\sqrt{T})\\ & + 2\,\sqrt{T}\,\exp\left(\frac{t}{2}\,(11 + 20C + \sqrt{T})\right)\\ & - 20C(-1 + \exp(t\,\sqrt{T})) \times (\sqrt{T}(1 + 24C))^{-1},\end{aligned} \qquad \textbf{[A2.3]}$$

where $T(t) = 101 + 40C(t)(-1 + 10C(t))$.

Appendix 3: Electric Fields Inside the Synaptic Clef. The membrane potential profile inside the synaptic cleft has been described in detail (24). In brief, the transmembrane voltage $V(r, t)$ inside and outside the receptor (active) zone follows the equations, respectively:

$$\frac{c_m}{2\pi r}\frac{\partial V}{\partial t} = \frac{\delta}{R_{ex}}\left(\frac{1}{r}\frac{\partial V}{\partial r} + \frac{\partial^2 V}{\partial r^2}\right) - \frac{\gamma N}{\pi r_a^2}V \quad r_a > r > 0 \qquad \textbf{[A3.1]}$$

$$\frac{c_m}{r}\frac{\partial V}{\partial t} = \frac{2\pi\delta}{R_{ex}}\left(\frac{1}{r}\frac{\partial V}{\partial r} + \frac{\partial^2 V}{\partial r^2}\right) \quad R > r > r_a, \qquad \textbf{[A3.2]}$$

where c_m is the membrane capacitance calculated per unitary radial increment at distance r from the center and R_{ex} stands for the extracellular medium unit resistance.

In accordance with classical physics, the value of R_{ex} can be related to the diffusivity of the corresponding ion species through the expression

$$R_{ex} = \frac{R_g T}{F^2 \sum_i D_i z_i^2 C_i}, \qquad \textbf{[A3.3]}$$

where R_g is the gas constant, T is absolute temperature, F is the Faraday's constant, and D_i, z_i, and C_i stand for the diffusion coefficient, valence, and concentration of the ion species in question. Assuming that diffusion retardation of small glutamate molecules in the cleft (compared with free medium) is similar to that of other small ions, R_{ex} and D could be related through the simple expression $R_{ex} = R_{free} D_{free}/D$, where R_{free} and D_{free} stand for the known values of, respectively, electrolyte resistance and glutamate diffusivity in a free medium.

In the common case of steady-state approximation (where spatial relaxation of the electrical field is much faster than diffusion), the radial voltage profile in the cleft follows the expressions

$$V(r) = V_o \frac{I_0(r/\lambda)}{I_0(L) + LI_1(L)\ln(R/r_a)}, \quad r_a > r > 0 \qquad \textbf{[A3.4]}$$

$$V(r) = V_o \frac{I_0(L) + LI_1(L)\ln(r/r_a)}{I_0(L) + LI_1(L)\ln(R/r_a)}, \quad R > r > r_a,$$

where I is the modified Bessel function, $L = \sqrt{\gamma N R_{ex}/\pi\delta}$, $\lambda = r_a/L$, V_o is the resting membrane voltage outside the cleft, and $\gamma = 25$ pS stands for the single receptor conductance. Expression **A3.4** assumes zero reversal potential for AMPA receptors.

Appendix 4: Monte Carlo Simulations. Here we used the same synaptic environment as above, with the flat cylindrical cleft surrounded by a free medium (Fig. 1*A*). Q glutamate molecules were released instantaneously in the synaptic cleft center. Movements of each molecule followed the three-dimensional random (Brownian) walk trough elementary displacements $\Delta = \sqrt{6Ddt}$, where dt is the time step and D is the diffusion coefficient. The value of dt was adjusted so that Δ was in the region of 1–2 nm. Individual molecules could move along any of the three Euclidean axes with the same probability in each direction ($\pm x$, $\pm y$, $\pm z$). Reflections from cell walls represented nonslip elastic interactions.

To compute activation rates of AMPA receptors, we first calculated the local concentration of glutamate $C(t)$ in the $\delta_D = 1$ nm vicinity (comparable with the Debye radius) of the postsynaptic membrane. This gave $C(t) = N_\delta(2\pi r\delta_D\Delta r)^{-1}$, where N_δ stands for the number of molecules which happen to occur at time point t inside the ring of thickness δ_D, width Δr and radius r. The concentration of open receptors $[O](r)$ within the corresponding ring in the active zone (radius $r < r_a$, width Δr) was then calculated at each time step from the multistage AMPA receptor kinetic scheme (25) and the average concentration of AMPA receptors in the active zone, $N(\delta\pi r_a^2)^{-1}$. Following numerical integration, this gave the total synaptic current in the form of

$$I_{syn} = 2\pi \sum_{i=1}^{r_a/\Delta r} iV(r)\gamma(\Delta r)^2[O](r), \qquad \textbf{[A4.1]}$$

where $r_a/\Delta r$ was calculated to the nearest integer and the profile of $V(r)$ reflected the electrical impedance of the cleft, in accordance with **A3.3** and **A3.4**.

Appendix 5: Main Notations and Symbols. R, radius of the synaptic apposition zone (200–1,000 nm); δ, synaptic cleft height (explored between 5 and 40 nm); Q, the number of released neurotransmitter molecules (3,000–8,000); D, effective diffusion coefficient of glutamate in the cleft (0.15–0.50 μm^2/ms); D_{free}, diffusion coefficient of glutamate in a free aqueous medium ($\approx$1.0 μm^2/ms at 37°C); t, time variable; r, radial distance from the cleft centre (variable); N, total number of AMPA receptors within the active zone (50–200); r_a, radius of the synaptic active zone (70 nm); P_o, fraction of open receptors; V, local membrane potential; R_{ex}, extracellular medium resistivity inside the synaptic cleft (constrained parameter); R_{free}, resistivity of a free extracellular medium ($\approx$59 Ohm·cm at 35–37°C); I_{syn}, total synaptic current through open receptors; γ, conductivity of a single receptor-channel; V_o, the postsynaptic resting membrane potential outside the cleft; V_{rev}, the receptor reversal potential; J_0 and J_1, Bessel functions of the first kind; I_0 and I_1, modified Bessel functions; C, effective glutamate concentration; C^*, the average effective glutamate concentration within the active zone; c_m, membrane capacitance calculated per unitary radial increment; R_g, gas constant; T, absolute temperature; F, Faraday's constant.

D.A.R. was supported by Wellcome Trust, Medical Research Council (United Kingdom), European Union (PROMEMORIA LSHM-CT-2005–512012), and Human Frontier Science Program.

1. Stuart GJ, Hausser M (2001) *Nat Neurosci* 4:63–71.
2. Chadderton P, Margrie TW, Hausser M (2004) *Nature* 428:856–860.
3. Clements JD, Lester RAJ, Tong G, Jahr CE, Westbrook GL (1992) *Science* 258:1498–1501.
4. Bergles DE, Dzubay JA, Jahr CE (1997) *Proc Natl Acad Sci USA* 94:14821–14825.
5. Lehre KP, Rusakov DA (2002) *Biophys J* 83:125–134.
6. Franks KM, Stevens CF, Sejnowski TJ (2003) *J Neurosci* 23:3186–3195.
7. Nielsen TA, DiGregorio DA, Silver RA (2004) *Neuron* 42:757–771.
8. Wahl LM, Pouzat C, Stratford KJ (1996) *J Neurophysiol* 75:597–608.
9. Barbour B, Keller BU, Llano I, Marty A (1994) *Neuron* 12:1331–1343.
10. Cathala L, Holderith NB, Nusser Z, DiGregorio DA, Cull-Candy SG (2005) *Nat Neurosci* 8:1310–1318.
11. Ventura R, Harris KM (1999) *J Neurosci* 19:6897–6906.
12. Rusakov DA, Kullmann DM (1998) *J Neurosci* 18:3158–3170.
13. Sykova E, Chvatal A (1993) *J Chem Neuroanat* 6:247–260.
14. Hrabetova S, Hrabe J, Nicholson C (2003) *J Neurosci* 23:8351–8359.
15. Orosz A, Kovacs J, Madarasz E, Falus A, Adam G (1975) *Acta Biol Acad Sci Hung* 26:23–35.
16. Petit TL, LeBoutillier JC, Alfano DP, Becker LE (1984) *Exp Neurol* 83:13–23.
17. Markus EJ, Petit TL, LeBoutillier JC (1987) *Brain Res* 432:239–248.
18. Adams I (1987) *Brain Res* 424:343–351.
19. Peters A, Palay SL, Webster HDF (1991) *The Fine Structure of the Nervous System* (Oxford Univ Press, New York).
20. Tanaka H, Shan W, Phillips GR, Arndt K, Bozdagi O, Shapiro L, Huntley GW, Benson DL, Colman DR (2000) *Neuron* 25:93–107.
21. Phillips GR, Huang JK, Wang Y, Tanaka H, Shapiro L, Zhang W, Shan WS, Arndt K, Frank M, Gordon RE, *et al.* (2001) *Neuron* 32:63–77.

22. Zuber B, Nikonenko I, Klauser P, Muller D, Dubochet J (2005) *Proc Natl Acad Sci USA* 102:19192–19197.
23. Eccles JC, Jaeger JC (1958) *Proc R Soc London B* 148:38–56.
24. Savtchenko LP, Antropov SN, Korogod SM (2000) *Biophys J* 78:1119–1125.
25. Jonas P, Major G, Sakmann B (1993) *J Physiol* 472:615–663.
26. Edmonds B, Gibb AJ, Colquhoun D (1995) *Annu Rev Physiol* 57:495–519.
27. Clements JD, Feltz A, Sahara Y, Westbrook GL (1998) *J Neurosci* 18:119–127.
28. Trommershauser J, Marienhagen J, Zippelius A (1999) *J Theor Biol* 198:101–120.
29. Scott R, Rusakov DA (2006) *J Neurosci* 26:7071–7081.
30. Okada YC, Huang JC, Rice ME, Tranchina D, Nicholson C (1994) *J Neurophysiol* 72:742–753.
31. Baumann SB, Wozny DR, Kelly SK, Meno FM (1997) *IEEE Trans Biomed Eng* 44:220–223.
32. Shepherd GMG, Harris KM (1998) *J Neurosci* 18:8300–8310.
33. Nusser Z, Lujan R, Laube G, Roberts JDB, Molnar E, Somogyi P (1998) *Neuron* 21:545–559.
34. Takumi Y, Ramirez-Leon V, Laake P, Rinvik E, Ottersen OP (1999) *Nat Neurosci* 2:618–624.
35. Harris KM, Sultan P (1995) *Neuropharmacology* 34:1387–1395.
36. Oertner TG, Sabatini BL, Nimchinsky EA, Svoboda K (2002) *Nat Neurosci* 5:657–664.
37. Hausser M, Roth A (1997) *J Neurosci* 17:7606–7625.
38. Bliss TVP, Collingridge GL (1993) *Nature* 361:31–39.
39. Nicoll RA, Schmitz D (2005) *Nat Rev Neurosci* 6:863–876.
40. Segal M (2005) *Nat Rev Neurosci* 6:277–284.